Clutter Rejection Filters in Color Flow Imaging: A Theoretical Approach

Hans Torp, *Member, IEEE*

***Abstract*—A general class of linear clutter rejection filters is described, covering the commonly used filter types including FIR/IIR filters with linear initialization, as well as regression filters, where the clutter component is estimated by least square curve fitting. The filter can be described by a complex valued matrix, and a frequency response is defined. However, in contrast to a time invariant filter, the general linear filter may create frequency components which are not present in the input signal. This produces bias in the velocity and velocity spread estimates. It is shown that the clutter filter effect on the autocorrelation estimates can be described by a frequency domain transfer function, but unlike time invariant filters, the transfer function is different for each temporal lag of the autocorrelation function. Using a two dimensional (axial and temporal dimension) model of the received signal, the bias in velocity and velocity spread is quantified, both for the autocorrelation algorithm and the time shift crosscorrelation estimator. Theoretical expressions, as well as numerical examples are given.**

I. Introduction

Clutter rejection filters are known from radar applications, where the signals from stationary (or fixed) targets, commonly referred to as "ground clutter", must be suppressed in order to detect moving targets, like aircrafts etc. In the simplest form of this technique, the received back scattered signals from two consecutive pulses are subtracted so that the signals from stationary targets are removed. This is called a fixed target canceller (FTC) [1] . In ultrasound Doppler blood flow measurements, the blood signals are corrupted with clutter signals from muscular tissue, vessel walls etc. which are much stronger than the blood signals; the clutter-to-signal ratio may in some cases exceed 100 dB. Unlike in ground based radar, there is always a relative movement between the ultrasonic probe and the unwanted tissue targets due to the operator moving the hand held probe, and blood vessel wall pulsation. Tissue velocities are highest in the cardiac muscle where the peak velocity may exceed 10 cm/sec, whereas normal intracardiac blood velocities are in the range 0–60 cm/sec. In patients with valvular disease, the blood velocities in the jet stream can exceed 5 m/sec. For continuous and pulsed wave Doppler, a conventional highpass filter can be used for clutter rejection with sufficiently high stop-band damping, and steep slope between the stopband and the passband, to obtain optimal separation between the clutter and the blood signals. Both FIR and IIR filters are used, the latter is often preferred, because a steep filter edge can be obtained with less computation power.

Clutter filters for 2D color flow imaging require different solutions, depending on the scanning principle. Mechanical scanning systems have a continuous movement of the beam. The signal from each range gate gives a relatively long signal sequence as the beam sweeps over the image. A similar filter as that used for CW/PW Doppler may be used; one filter for each range gate. The only difference is that the beam movement gives an additional transit-time effect for the clutter signal, giving a slightly higher clutter bandwidth in the clutter signal. With phased array and linear array technique, the beam is moved stepwise over the image, transmitting a limited number of pulses in each direction. Each time the beam is moved to a new position, a discontinuity in the clutter signal occurs, which means that the clutter filter has to operate separately on the samples in each beam direction. The number of temporal samples available for the clutter filter is therefore equal to the number of transmitted pulses per beam, which must be kept low (typical values are 6–16 samples) in order to obtain a frame rate which is sufficient to follow the dynamic behavior in arterial, and intracardiac bloodflow.

A number of different approaches has been proposed for clutter rejection filtering operating on a small number of signal samples. A FIR filter with short impulse response is a possible solution, the number of output samples is then reduced according to the filter order. The simplest FIR clutter filter is the first order FTC filter, which is analyzed in [2]. IIR filters may also be used, if special precaution is taken to initialize the filter, in order to reduce the ring-down time. A simple IIR initialization technique is described in [3], but more sophisticated methods based on prediction of the clutter signal outside the observation interval have also been proposed [3]. A novel approach was taken by Hoeks [4], where the clutter signal was estimated by linear regression, and then subtracted from the input signal. The advantage of this technique is that the number of output samples is not reduced. Higher order polynomial regression filters have also been analyzed in [3].

The performance of a linear time invariant filter is adequately described by its frequency transfer function, which changes the shape of the Doppler spectrum. However, the effect of time variant filters, like the polynomial regression filter, is more complicated to describe. For applications in color flow imaging, the output of the filter undergoes autocorrelation analysis. The correlation both in time (pulse-to-pulse) and in space (along the ultrasonic beam) have

Manuscript received February 20, 1996; accepted August 10, 1996.

The author is with the Department of Physiology and Biomedical Engineering, Norwegian University of Science and Technology, Trondheim, Norway (e-mail: hanst@ibt.unit.no).

been used for the estimate of velocity and velocity spread [5], [6]. Therefore, the effect of the clutter filter on the estimates of the two-dimensional (axial and temporal) autocorrelation function should be considered. The aim of this work is to give a theoretical basis for the practical design of optimum clutter rejection filters. The paper is organized as follows:

Part II describes a model of the received ultrasonic signal after complex demodulation, including blood signal, clutter signal, and thermal noise. The signal is modeled as a two dimensional complex Gaussian process, described by the signal correlation function in depth-range, as well as correlation in time (from pulse to pulse). Two dimensional clutter rejection filters are discussed briefly, but in the rest of the work, only one-dimensional filters are analyzed. In part III the general one-dimensional linear clutter filter operating on a finite, time discrete complex valued signal is described mathematically. The frequency response is defined, and expressed by the filter matrix elements. In part IV the clutter filter effect on the two dimensional autocorrelation function estimate is described. Analytical expressions for the bias in estimates of velocity and velocity spread are derived, and some numerical examples are given.

II. Model for the Received Ultrasonic Signal

A signal model which includes both temporal (pulse-to-pulse) correlation, as well as spatial correlation is needed in order to analyze the behavior of the large variety of velocity estimators proposed [5], [6]. Stochastic models for ultrasound color flow imaging have been presented by a number of authors [7]–[9]. Here, the model description is taken from a previous work [10], where the received signal after complex demodulation is described as a two-dimensional complex Gaussian process $x(t,k)$. In this notation t is the elapsed time from pulse transmission k, corresponding to a depth range $r = ct/2$. In a practical implementation, the signal in digital form is only available for discrete samples in range, however the sampling frequency can be arbitrary high. If the baseband signal is sampled with a frequency higher than the bandwidth, any value in between can be found by interpolation. In the following analysis, the signal is assumed to be a continuous function of t, the elapsed time after pulse transmission, and discrete in the second parameter k. The pulse repetition time is denoted T. As a stationary, complex Gaussian process, the signal is completely characterized by its autocorrelation function, or its power spectrum which are defined as

$$\begin{aligned} R_{xx}(\tau, m) &\equiv \langle x(t,k)^* x(t+\tau, k+m)\rangle \\ G_{xx}(\omega_1, \omega_2) &\equiv \sum_m \int d\tau R_x(\tau, m) e^{i\omega_1 \tau} e^{i\omega_2 mT}. \end{aligned} \quad (1)$$

The angular frequency variables ω_1 and ω_2 are the ultrasound frequency (in the MHz range), and the Doppler frequency (in the kHz range). The autocorrelation function is defined by a statistical ensemble average. In a practical estimator, ensemble averaging must be replaced by radial and/or temporal (pulse-to-pulse) averaging, to reduce variance. The stationary assumption in (1) is only valid in a limited depth range, and for short observation times.

When all scatterers within the sample volume move with the same velocity, the two-dimensional autocorrelation function and power spectrum takes on the form [11]

$$\begin{aligned} R_{xx}(\tau, m; v_r, v_t) &= s_2\left(\tau - \frac{2v_r T}{c} m\right) e^{-i\omega_0 \tau} b_2(v_t T m) \\ G_{xx}(\omega_1, \omega_2; v_r, v_t) &= |S(\omega_1 + \omega_0)|^2 \sum_n \left| B\left(\frac{1}{v_t} \right.\right. \\ &\quad \times \left.\left.\left(\omega_2 - \frac{2v_r}{c}(\omega_1 + \omega_0) + \frac{2\pi}{T} n\right)\right)\right|^2. \end{aligned} \quad (2)$$

$S(\omega_1)$ and $B(\omega_2)$ are the Fourier transform of the transmitted pulse, and the transversal beam profile, respectively, and ω_0 is the angular demodulation frequency. The blood velocity vector is described by the radial (along the ultrasonic beam) component v_r, and the transversal component v_t. Frequency dependent attenuation and scattering are included in the pulse response $S(\omega_1)$. Note that the power spectrum $G(\omega_1, \omega_2)$ is periodic in the second frequency parameter, with period $2\pi/T$.

Both the clutter signal and the blood signal may consist of several independent components, moving with different velocities, each of them contributing with a power spectrum having the form described in (2). Significant acceleration during the observation time, or turbulence will increase the bandwidth further in the ω_2 direction. Thermal noise from the transducer and receiver front end amplifier adds an independent white noise component to the signal. In order to optimize the signal-to-noise ratio, the receiver bandwidth is usually matched to the pulse bandwidth, by a bandpass filter centered around ω_0, and/or a lowpass filter after the complex demodulation stage. The total receiver filter is here described by a bandpass impulse response $h(\tau)$. The autocorrelation function and the power spectrum for the received signal will be a sum of these independent components:

$$\begin{aligned} R_{xx}(\tau, m) &= \sum_n A_n R(\tau, m; \underline{v}_n) + N_0 h_2(\tau) e^{-i\omega_0 \tau} \delta(m) \\ G_{xx}(\omega_1, \omega_2) &= \sum_n A_n G(\omega_1, \omega_2; \underline{v}_n) + N_0 |H(\omega_1 + \omega_0)|^2. \end{aligned} \quad (3)$$

The last term in (3) accounts for the thermal noise, which is a lowpass process, with spectral energy density N_0, and spectral shape given by the transfer function $H(\omega_1 + \omega_0)$. An illustration of a typical 2D power spectrum, including blood signal, clutter signal, and thermal noise is shown in Fig. 1. Note that the signal spectrum is concentrated along straight lines in the (ω_1, ω_2)-plane, intersecting the ω_1 axis at $\omega_1 = -\omega_0$, each with a slope proportional to the velocity. These lines are referred to as iso-velocity lines.

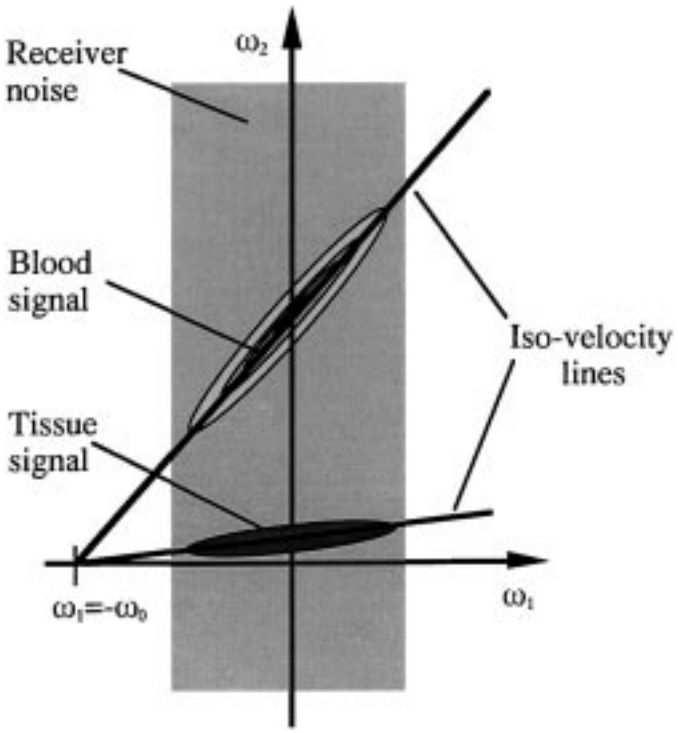

Fig. 1. Two dimensional power spectrum including components from blood signal, tissue signal, and receiver noise.

An ideal clutter rejection filter should therefore suppress all frequency components below the iso-velocity line given by the highest tissue velocity. This means that the filter cut-off frequency should increase with ω_1. However, the difference in frequency dependent scattering from blood and clutter will alter this: Raleigh scattering from blood [7] gives increased intensity in the higher frequency components, which means that the blood/clutter level increases with the frequency ω_1. This means that the stopband rejection requirement is less, and a lower cutoff frequency can be used for the higher frequency components. Thus the optimum 2D frequency response for the clutter filter, depends on the actual blood/clutter level. A one dimensional clutter filter, for which the cutoff frequency is independent of ω_1, seems to be a useful compromise. This is also preferred for real-time processing, since the computation requirements are much higher for a 2D filter. The following analysis is restricted to one dimensional clutter rejection filters.

III. The General Linear Clutter Rejection Filter

In this section, the filter effect on each range sample of the received signal is analyzed separately. The input and output of the filter is a sequence of N complex signal samples, from one selected range gate of the received signal. A general clutter rejection filter can be described mathematically as a transform on the N dimensional complex vector space $\mathbf{C}^N$. To avoid intermodulation between the different clutter and blood components in the output signal, the transform should be linear, and can therefore be performed by a matrix multiplication. Note that the general linear transform includes all types of conventional time invariant filters. IIR filters can also be described in this way, if the initialization of the filter is performed by a linear combination of the input signal samples. The filter matrix $A = \{a(n,m)\}$ may have complex entries, when a skewed (non symmetric) frequency response is required.

$$\begin{aligned} &\text{Input vector: } \underline{x} = (x(1), \ldots, x(N))^T \\ &\text{Output Vector: } \underline{y} = (y(1), \ldots, y(N))^T = A\underline{x} \\ &y(k) = \sum_{n=1}^{N} a(k,n)x(n); \quad k = 1, \ldots, N. \end{aligned} \tag{4}$$

A time invariant FIR filter with an impulse response $h(n)$, $n = 0, 1, \ldots, M$ will have a filter matrix given by:

$$a(k,n) = \begin{cases} h(k-n) & \text{for } k \geq n \text{ and } k > M \\ 0 & \text{elsewhere.} \end{cases}$$

Note that the first M samples in the output signal are zero. The frequency response of the FIR filter can be defined by the Fourier transform of the impulse response $h(n)$. This definition can not be applied to the general linear filter (4). However, a frequency response function $H_0(\omega)$ can be defined as the power of the output signal when the input is a complex harmonic signal.

$$\begin{aligned} x(k) &= e^{ik\omega}; \quad k = 1, 2, \ldots, N \\ y\omega(k) &= \sum_{n=1}^{N} a(k,n)e^{-in\omega} \equiv A_k(-\omega) \\ H_0(\omega) &\equiv \frac{1}{N}\sum_{k=1}^{N} |y_\omega(k)|^2 = \frac{1}{N}\sum_{k=1}^{N} |A_k(-\omega)|^2. \end{aligned} \tag{5}$$

The quantity $A_k(\omega)$ is the Fourier transform of row number k in the filter matrix. Since the transform is linear, a constant phase shift of the input signal will give a factor $e^{i\phi}$ with unit length, and will therefore not influence the output power. This means that the frequency response in (5) is well defined. This is a unique property for complex baseband signals. For real valued signals, an ensemble average over all possible phases is necessarily in order to obtain a well defined frequency response [4]. In the complex case, the power of the real- and imaginary parts both vary with the phase of the input signal in such a way that the sum is constant. Note that for FIR filters, the frequency response defined in (5) coincide with the usual definition; i.e., the squared Fourier transform of the impulse response $h(n)$. However, unlike the linear convolution filter, the output will not in general be a complex harmonic sequence, but may contain frequency components which are not present in the input signal. This property can cause severe problems in color flow imaging, where strong clutter signals may generate higher frequency components which affect both the center frequency and the bandwidth estimate.

This frequency distortion is only absent for FIR-filters, where the number of non-zero output samples must be reduced to $N - M$, where M is the FIR filter order. A reduction of the number of output samples will increase the variance in the velocity parameter estimates, and should therefore be minimized. Several methods have been proposed for reducing the "ring-down time" in the filter [3]. The basic idea is to extend the signal interval by some sort of prediction, followed by a FIR or IIR convolution filter. As long as the predicted values are formed by linear combinations of the original input signal, the total filter operation will still be linear, and thus included in the general class of filters (4), which can be performed by a matrix multiplication.

Another approach was taken by Hoeks et. al [4], where the clutter signal was estimated by least square fitting of the signal to a straight line, and then subtracted from the input signal. This is one example from a class of filters which here will be referred to as *regression filters*. If we assume that the clutter signal is contained in a subspace κ of $\mathbf{C}^N$, the projection transform P_κ from $\mathbf{C}^N$ onto κ gives the least square fit to the clutter component. The clutter filter will then have the form $A = I - P_\kappa$, which is a projection into the orthogonal complement of κ. If $\{b_0, b_1, \ldots, b_P\}$ is an orthonormal basis for κ, the filter operation can be performed by calculating the projection along each basis vector, and subtract the projections from the original signal. The filter matrix $\{a(n,m)\}$ and the frequency transfer function for the regression filter have the following form:

$$a(n,m) = \delta(n-m) - \sum_{p=0}^{P} b_p(n)^* b_p(m)$$

$$H_0(\omega) = 1 - \frac{1}{N}\sum_{p=0}^{P} |B_p(\omega)|^2 \qquad (6)$$

$$B_p(\omega) \equiv \sum_{n=1}^{N} b_p(n) e^{-in\omega}.$$

The choice of basis functions $\{b_0, b_1, \ldots, b_P\}$ determines the regression filter properties. The Legendre polynomials form a set of basis functions which is suitable for clutter rejection filters, due to the high stopband rejection. The Legendre polynomials can be obtained by applying the Gram-Schmidt orthonormalization process to the series of polynomials $\{1, n, n^2, \ldots, n^P\}$. In Fig. 2 the frequency responses for the Legendre polynomials and the resulting regression filter are shown, for $N = 10$, and $p = 0, 1, 2, 3$. The corresponding clutter rejection filter is equivalent to a least square polynomial fit of order P to the clutter component. Note that the basis functions are real valued, giving a symmetric frequency response. Fig. 3 shows the frequency responses for the polynomial regression filter, for different orders P.

It is interesting to see how the clutter filter affects the power spectrum estimate of the output signal. A smooth weighting function on the output signal can be included

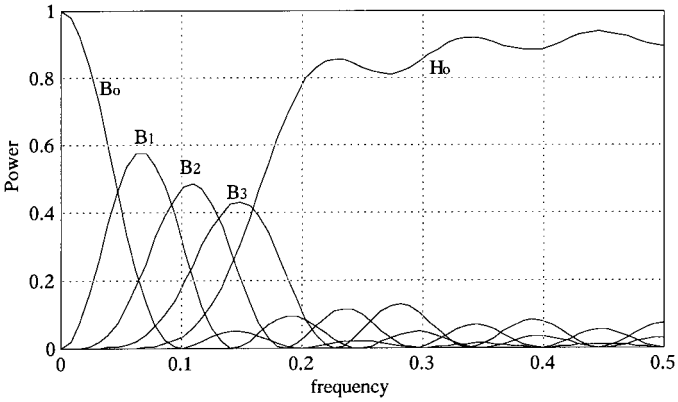

Fig. 2. Frequency spectra for the Legendre polynomials, $|B_p|^2$ for $p = 0, 1, 2, 3$ and the frequency response for the 3rd order polynomial regression filter. $N = 10$. All frequencies in the figures are represented as fractions of the sampling rate.

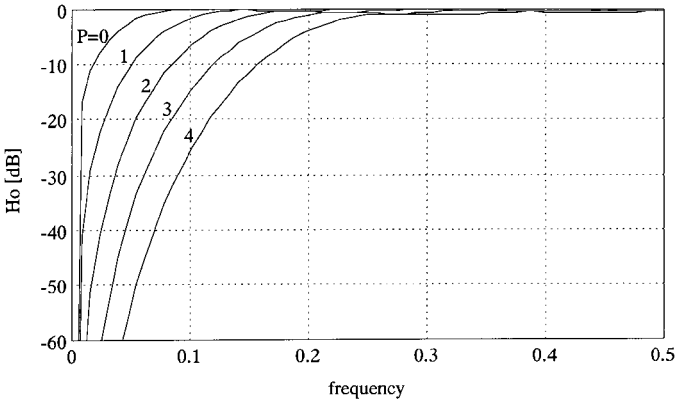

Fig. 3. Frequency response for the Legendre polynomial regression filter, with order $P = 0, 1, 2, 3$, and 4. $N = 10$.

in the filter matrix coefficients. If the input signal power spectrum is $G_{xx}(\omega)$, the expected output spectrum is

$$\langle \hat{G}_{yy}(\omega) \rangle = \int d\zeta |A(\zeta,\omega)|^2 G_{xx}(\zeta)$$

$$A(\zeta,\omega) \equiv \sum_{k,m} a(k,m) e^{-i(k\zeta + m\omega)}. \qquad (7)$$

This equation shows that the two-dimensional Fourier transform $A(\zeta,\omega)$ of the filter matrix can be interpreted as a power spectrum transfer function. A single frequency input $G_{xx}(\omega) = \delta(\omega - \omega_1)$, gives the output spectrum $G_{yy}(\omega) = |A(\omega_1,\omega)|^2$. In Fig. 4 the spectrum transfer function for a 4th order polynomial regression filter with Hanning window, $N = 20$ is shown. Note the increase in side lobe level, when the input frequency is close to the filter cut-off frequency. This example illustrates that frequency distortion in polynomial regression filters is only significant for input frequencies at and below the filter cutoff frequency.

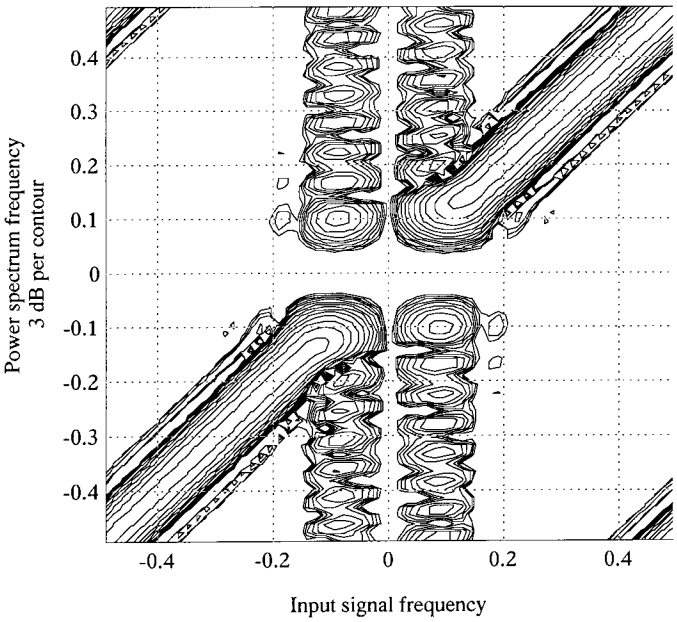

Fig. 4. The spectrum transfer function $|A(\omega_1, \omega_2)|^2$ for $N = 20$ point Hanning window, and 4th order regression filter. The contours are drawn at 3 dB distance over 40 dB dynamic range.

IV. Clutter Rejection Filter Effect on the Autocorrelation Estimate

In color flow imaging applications, the output signal from the clutter filter is used for autocorrelation analysis to derive blood velocity information. In this section, the behavior of the autocorrelation estimate for the output of a general linear filter is studied. The unbiased sample mean autocorrelation estimate of the received Doppler signal described in section II is given by

$$\hat{R}_{yy}(\tau, m) = k(\tau, m) \int_{t=t_0}^{t_0+T_0-\tau} dt \sum_k y(t,k)^* y(t+\tau, k+m)$$
$$y(t,k) = \sum_{n=1}^{N} a(n,k) x(t,n); \quad k(\tau,m) \equiv \frac{1}{T_0 - \tau} \frac{1}{N-m}. \tag{8}$$

By combining the two equations in (8), the expected value for the autocorrelation estimate can be expressed by the input autocorrelation function and the filter matrix coefficients $\{a(m,n)\}$. Details can be found in the appendix. Note that the output signal is not in general a stationary process, even though the input signal is assumed to be stationary.

$$\langle \hat{R}_{yy}(\tau, m) \rangle = \sum_n a_2(n,m) R_{xx}(\tau, n)$$
$$a_2(n,m) \equiv \sum_{m',n'} a(n',m')^* a(n'+n, m'+m). \tag{9}$$

Equation (9) shows that the autocorrelation functions $\{R(\tau,m)\}_{m=0,\pm1,\ldots\pm N}$ for the input signal and the output signal are related by a linear transformation, and that the transformation matrix is the (two-dimensional) autocorrelation of the filter matrix. The autocorrelation function for y can also be expressed by the power spectrum of the input signal, $G_{xx}(\omega_1, \omega_2)$

$$\langle \hat{R}_{yy}(\tau, m) \rangle = \iint d\omega_1 d\omega_2 G_{xx}(\omega_1, \omega_2) H_m(\omega_2) e^{i\tau\omega_1 + im\omega_2}$$
$$H_m(\omega_2) \equiv \frac{1}{|N-m|} \sum_n a_2(n+m, m) e^{in\omega_2}. \tag{10}$$

This shows that the filter can be described by a set of transfer functions, $\{H_m(\omega)\}$, one for each temporal lag m in the autocorrelation estimate. In general, the transfer functions $H_m(\omega)$ are different for each value of the temporal lag parameter m, and attain complex values when $m \neq 0$. The transfer functions may also be expressed by the Fourier transform of the filter matrix elements

$$H_m(\omega_2) = \frac{1}{|N-m|} \sum_k A_k(\omega_2)^* A_{k+m}(\omega_2) e^{-im\omega_2}$$
$$A_k(\omega_2) \equiv \sum_n a(n,k) e^{-in\omega_2}. \tag{11}$$

The function $A_k(\omega)$ is the Fourier transform of row number k in the filter matrix. In Fig. 5, the magnitude of the transfer functions H_0, H_1, and H_5 are plotted for a 3rd order polynomial regression filter.

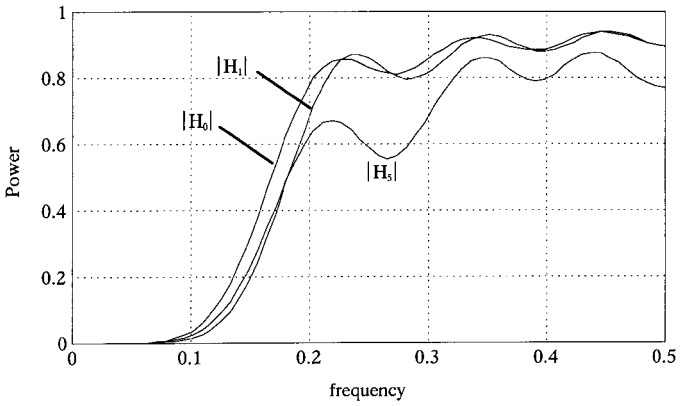

Fig. 5. Magnitude of the frequency transfer functions H_m for $m = 0$, 1, and 5. Third order polynomial filter, with $N = 10$.

For time invariant filters, $A_k(\omega) = H(\omega) e^{-ik\omega}$, where $H(\omega)$ is the ordinary filter transfer function, and the transfer functions for the different lags coincide.

$$H_m(\omega) = \frac{1}{|N-m|} \sum_k (H(\omega) e^{ik\omega})^* H(\omega) e^{i(k+m)\omega} e^{-im\omega}$$
$$= |H(\omega)|^2. \tag{12}$$

For applications in color flow imaging, the signal power, velocity and velocity spread are usually calculated from the autocorrelation estimates with temporal lags $m = 0$ and $m = 1$. By normalizing the autocorrelation function with

temporal lag $m = 1$, a correlation coefficient is obtained.

$$\text{Signal power: } \hat{R}_{yy}(0,0)$$
$$\text{Correlation coefficient: } \hat{\rho}(\tau,1) = \frac{\hat{R}_{yy}(\tau,1)}{\hat{R}_{yy}(0,0)} \tag{13}$$

The most commonly used method, the "autocorrelation method" [12] utilizes only spatial lag $\tau = 0$; the velocity and velocity spread are given by the phase and magnitude of $\rho(0,1)$.

$$\text{Velocity: } v = \frac{c}{2\omega_0 T}\arg\{\rho_{yy}(0,1)\}$$
$$\text{Velocity spread: } 1 - |\rho_{yy}(0,1)| \tag{14}$$

The velocity can also be calculated from the pulse-to-pulse time delay shift [5], which can be found by the peak in the RF signal correlation function with temporal lag $m = 1$. The RF signal correlation function is obtained by upmixing of the baseband correlation function [13]

$$\text{peak}_\tau(\text{real}\{R_{yy}(\tau,1)e^{i\omega_0\tau}\}) \tag{15}$$

The effect of the clutter filter on both these color flow algorithms is determined by the transfer functions $H_0(\omega_2)$ and $H_1(\omega_2)$. Magnitude variation in the transfer functions over the Doppler signal bandwidth will give bias in all three velocity parameters. This is a well known effect, which is also present for time invariant filters. However, a nonzero phase value of $H_1(\omega_2)$ will give an additional bias in the velocity estimate. If the magnitude of the two transfer functions H_0 and H_1 are different, this will give an additional bias in the velocity spread estimate.

To evaluate these effects in more detail, the autocorrelation model (3) from section II is inserted in (10). Due to the linear relationship between the input and output autocorrelation function (10), each component in (3) can be treated separately. The signal component from blood moving with velocity $\underline{v} = (v_r, v_t)$ gives the following expected autocorrelation function

$$\begin{aligned}\langle\hat{R}_{yy}(\tau,m)\rangle &= e^{-i\omega_0\tau}\sum_k s_2\left(\tau - \frac{2v_rT}{c}k\right)b_2(v_tTk)a_2(k,m)\\ &= \int d\omega_1|S(\omega_1)|^2 e^{i\tau(\omega_1-\omega_0)}\int_0^{2\pi} d\omega_2 \sum_n \\ &\left|B\left(\frac{1}{v_t}\times\left(\omega_2 - \frac{2v_rT}{c}\omega_1 + 2\pi n\right)\right)\right|^2 H_m(\omega_2)e^{im\omega_2}\end{aligned} \tag{16}$$

When the transversal velocity components is zero, the B() function (which is the Fourier transform of the ultrasound beam profile) approaches a delta function, and (16) simplifies to

$$\begin{aligned}\langle\hat{R}_{yy}(\tau,m)\rangle &= e^{-i\tau\omega_0}\int d\omega_1|S(\omega_1)|^2 H_m\left(\frac{2v_rT}{c}\omega_1\right)\\ &\quad\times e^{i(\tau+m\frac{2v_rT}{c})\omega_1}\\ &\approx H_m\left(\frac{2v_rT}{c}\omega_0\right)e^{im\frac{2v_rT}{c}\omega_0}\end{aligned} \tag{17}$$

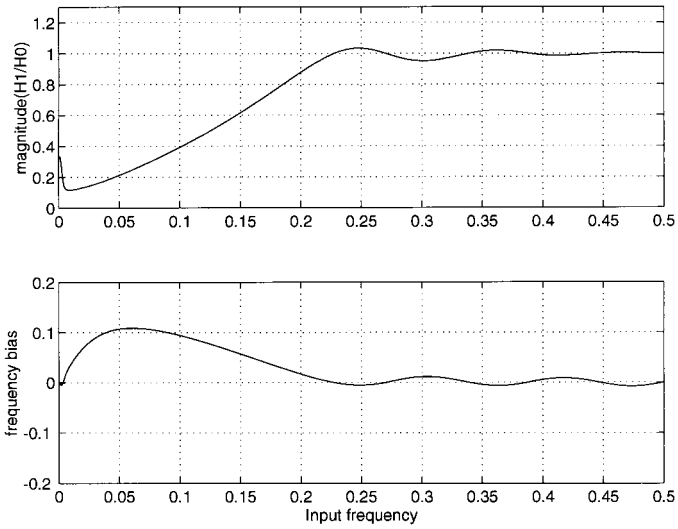

Fig. 6. Magnitude and phase of $H_1(\omega)/H_0(\omega)$ as a function of $\omega/2\pi$. Polynomial regression filter with $N = 10$, $P = 3$.

The last approximation in (17) is valid when the transmitted pulse bandwidth is much lower than the center frequency. In this case, the expected velocity and velocity spread are given purely by the clutter filter transfer functions. The normalized autocorrelation estimate takes on the simple form

$$\begin{aligned}\langle\hat{\rho}_{yy}(0,1)\rangle &\approx \frac{\langle\hat{R}_{yy}(0,1)\rangle}{\langle\hat{R}_{yy}(0,0)\rangle} \approx \frac{H_1(\omega)}{H_0(\omega)}e^{i\omega}\\ &= \frac{|H_1(\omega)|}{H_0(\omega)}e^{i\omega + i\arg\{H_1(\omega)\}}\\ \omega &= \frac{2v_rT}{c}\omega_0\end{aligned} \tag{18}$$

Observe that the phase of $H_1(\omega)$ determines the bias of the velocity estimate, whereas the fraction $|H_1/H_0|$ determines the bias of the velocity spread estimate. In Fig. 6 the magnitude and phase of $H_1(\omega)/H_0(\omega)$ is plotted for a polynomial regression filter of order 3. Note that the estimator bias is substantial in the stop band and in the transition region for both estimators.

For the time delay estimation algorithm, the RF autocorrelation function with temporal lag $m = 1$ is used, see (15). The expected value for the RF-correlation function, for uniform velocity fields in the presence of noise, is found from (2) and (16)

$$\begin{aligned}\langle\hat{R}_{yy}(\tau,1)e^{i\tau\omega_0}\rangle &= \sum_k s_2\left(\tau - \frac{2v_r}{c}kT\right)b_2(v_tkT)a_2(k,1)\\ &\quad + N_0h_2(\tau)a_2(0,1)\end{aligned} \tag{19}$$

Fig. 7 shows the effect of the clutter filter on the RF correlation function for a velocity at 0.35 times the Nyquist limit. The clutter filter changes both the waveform, and the position of the peak in the correlation function. The main correlation peak has been moved to the right, and the peak amplitude has been reduced, so that the subsidiary

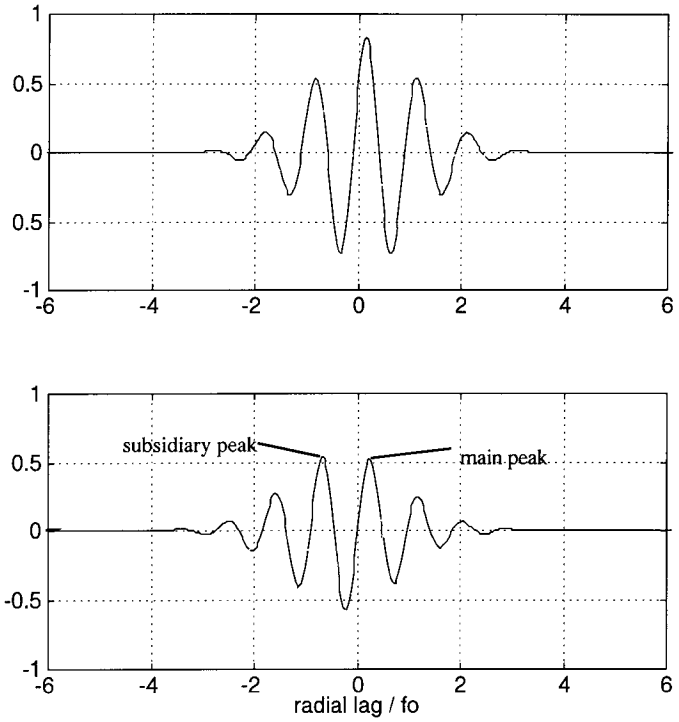

Fig. 7. The effect of polynomial regression filter to the RF crosscorrelation function. Upper plot is without filter, and lower plot is with a 3rd order filter. $N = 8$. $SNR = 10$ dB, $v = 0.35$*Nyquist limit.

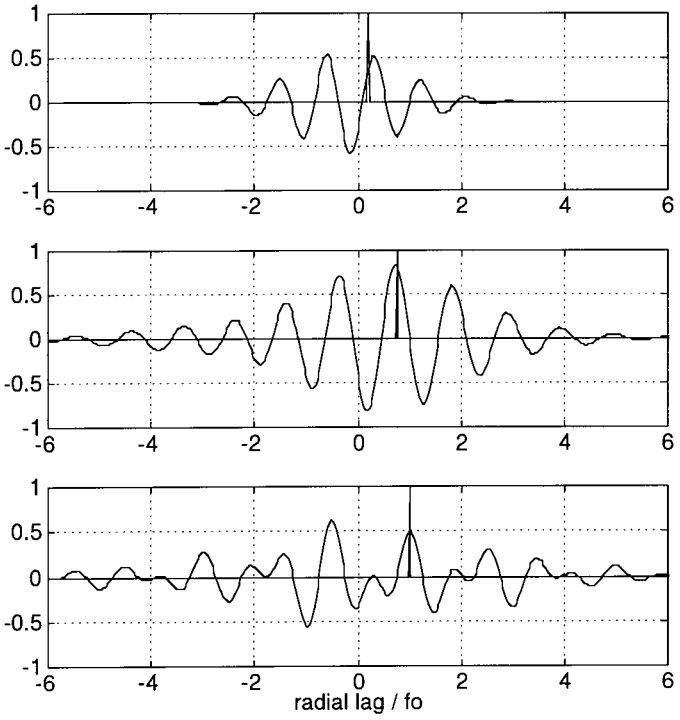

Fig. 8. The effect of polynomial regression filter to the RF crosscorrelation function, for three different velocities: 0.35 (upper), 1.5 (middle), and 2.0 (lower). The spike shows the correct peak position. Same filter as in Fig. 7.

peak to the left is higher. This will give an error in the velocity estimate equal to double the Nyquist velocity. In Fig. 8, the RF correlation function for three different velocities are compared. The correlation length is increased due to the clutter filter for all three velocities, but this gives no bias for the $v = 1.5$ case. The worst case situation occurs when the Doppler shift is at a multiple of the PRF, giving a destroyed waveform, and substantial bias in the velocity estimate.

V. Discussion and Conclusions

In this work, linear clutter filters applied to time discrete Doppler baseband signals of short duration have been described by a filter matrix, which can be complex in general. By using the complex signal formalism, the frequency response for the signal power is well defined, even for time variant filters.

The two-dimensional Fourier transform of the filter matrix gives the relation between the expected power spectrum of the input and the output signal of the filter. Increased side lobe level is observed for frequencies close to the filter cutoff frequency.

For autocorrelation analysis of the filter output signal, the filter effect is described by a sequence of (frequency domain) transfer functions, one for each temporal lag in the autocorrelation function. In general, the transfer functions may attain complex values for nonzero time lag. For time invariant filters, the transfer functions are all real valued, and equal to the squared frequency response, defined in the usual way as the Fourier transform of the impulse response.

Most color flow imaging algorithms are based on center frequency and bandwidth estimates derived from the first two temporal lags ($m = 0$ and $m = 1$) of the autocorrelation function. A non-zero phase of the transfer function H_1 gives a center frequency bias, whereas a difference in magnitude between H_0 and H_1 gives a bias in the estimated bandwidth. The example in Fig. 5 shows that the bandwidth estimate has substantial positive bias for frequency components below the filter cutoff frequency. This may give severe artifacts in a color flow image, in that low frequency clutter signals which have not been completely removed by the clutter filter, give high values in the bandwidth estimate, and may be interpreted as turbulent blood flow. Clutter filter design should therefore include the following optimization criteria:

a. The phase of H_1 should be as small as possible in the filter pass band.
b. The magnitude of the ratio H_1/H_0 should be close to unity in the transition band and the pass band.

Crosscorrelation time shift estimators have also been analyzed with respect to clutter filter effects. Generally, the clutter filter tends to increase the length of the crosscorrelation function in the range direction. Severe distortion of the correlation waveform has been observed when part of the signal bandwidth coincide with the stop band or transition band of the filter.

References

[1] R. Nitzberg, *Adaptive Signal Processing for Radar*: Artec House Inc., 1992.

[2] J. A. Jensen, "Stationary echo cancelling in velocity estimation by time-domain cross-correlation," *IEEE Trans. Med. Imag.*, vol. 12, no. , pp. 471–477, 1993.

[3] A. Kadi and T. Loupas, "On the performance of Regression and step-initialized IIR Clutter filters for color Doppler systems in diagnosing medical ultrasound," *IEEE Trans. Ultrason., Ferroelect., Freq. Contr.*, vol. 42, no. 5, pp. 927–937, 1995.

[4] A. P. Hoeks, J. J. van-de-Vorst, A. Dabekaussen, P. J. Brands, and R. S. Reneman, "An efficient algorithm to remove low frequency Doppler signals in digital Doppler systems," *Ultrason. Imaging*, vol. 13, no. 2, pp. 135–44, 1991.

[5] O. Bonnefous and P. Pesqué, "Time domain formulation of Pulse-Doppler Ultrasound and Blood Velocity Estimation by Cross-Correlation," *Ultrason. Imaging*, vol. 8, pp. 73–85, 1986.

[6] Ferrara and Algazi, "A new wideband spread target maximum likelihood estimator for blood velocity estimation—Part I: Theory," *IEEE Trans. Ultrason., Ferroelect., Freq. Contr.*, vol. UFFC-38, no. 1., pp. 1–26, 1991.

[7] B. A. J. Angelsen, "A theoretical study of the scattering of ultrasound from blood," *IEEE Trans. Biomed. Eng.*, vol. BME-27, no. 2, pp. 61–67, 1980.

[8] L. Y. Mo and R. S. Cobbold, "A unified approach to modeling the backscattered Doppler ultrasound from blood," *IEEE Trans. Biomed. Eng.*, vol. 39, no. 5, pp. 450–61, 1992.

[9] L. S. Wilson, "Description of Broadband Pulsed Doppler Ultrasonic Processing using the Two-Dimensional Fourier Transform," *Ultrason. Imaging*, vol. 13, pp. 301–315, 1991.

[10] H. Torp, K. Kristoffersen, and B. Angelsen, "Autocorrelation Techniques in Color Flow Imaging. Signal model and statistical properties of the Autocorrelation estimates," *IEEE Trans. Ultrason., Ferroelect., Freq. Contr.*, vol. 41, no. 5, pp. 604–612, September 1994.

[11] H. Torp and K. Kristoffersen, "Velocity Matched Spectrum Analysis: A new Method for suppressing Velocity Ambiguity in Doppler Sonogram," *Ultrasound in Medicine and Biology*, vol. 21, no. 7, pp. 937–944, 1995.

[12] C. Kasai, K. Namekawa, A. Koyano, and R. Omoto, "Real-Time Two-Dimensional Blood Flow Imaging Using an Autocorrelation Technique," *IEEE Trans. Sonics Ultras.*, vol. SU-32, no. 3, pp. 458–464, May 1985.

[13] H. Torp, X. Lai, and K. Kristoffersen, "Comparison Between Cross-correlation and Auto-correlation Technique in Color Flow Imaging," presented at IEEE Ultrasonic Symposium, Baltimore, Maryland, USA, 1993.

Appendix

Here the development of equation (9) and (10) are shown, which give the relation between the autocorrelation function for the filter input and output signal. The sample mean autocorrelation estimate of the filter output can be expressed by the input signal and the filter coefficients by combining the two expressions in (8)

$$\begin{aligned}\hat{R}_{yy}(\tau,m) &= \int dt \sum_k y(t,k)^* y(t+\tau,k+m) \\ &= \int dt \sum_k \sum_{n,m'} a(k,n)^* x(t,n)^* a(k+m,m') x(t+\tau,m') \\ &= \int dt \sum_{m'} \sum_{n,k} a(k,n) a(k+m,n+m')^* x(t,n)^* \\ &\quad \times x(t+\tau,n+m')\end{aligned} \tag{A1}$$

Taking the expected values of (A1), equation (9) is obtained

$$\begin{aligned}\langle \hat{R}_{yy}(\tau,m)\rangle &= \int dt \sum_{m'} \sum_{n,k} a(k,n) a(k+m,n+m')^* \\ &\quad \times \langle x(t,n)^* x(t+\tau,n+m')\rangle \\ &= \sum_{m'} R_{xx}(\tau,m') \sum_{n,k} a(k,n) a(k+m,n+m')^* \\ &= \sum_{m'} R_{xx}(\tau,m') a_2(m',m)\end{aligned} \tag{A2}$$

The frequency domain version of this equation is obtained by substituting R_{xx} with the 2-D Fourier transform of the power spectrum, equation (1) in paragraph II, in (A2)

$$\begin{aligned}\langle \hat{R}_{yy}(\tau,m)\rangle &= \frac{1}{|N-m|} \sum_n \iint d\omega_1 d\omega_2 G_{xx}(\omega_1,\omega_2) e^{i\tau\omega_1 + in\omega_2} \\ &\quad \times a_2(n,m) \\ &= \iint d\omega_1 d\omega_2 G_{xx}(\omega_1,\omega_2) \frac{1}{|N-m|} \sum_n a_2(n,m) \\ &\quad \times e^{i(n-m)\omega_2} e^{i\tau\omega_1 + im\omega_2} \\ &= \iint d\omega_1 d\omega_2 G_{xx}(\omega_1,\omega_2) H_m(\omega_2) e^{i\tau\omega_1 + im\omega_2} \\ H_m(\omega_2) &\equiv \frac{1}{|N-m|} \sum_n a_2(n,m) e^{i(n-m)\omega_2} \\ &= \frac{1}{|N-m|} \sum_n a_2(n+m,m) e^{in\omega_2}\end{aligned} \tag{A3}$$

Hans G. Torp (M'93) was born in Sarpsborg, Norway, in 1953. He received the M.S. and Dr.Techn. degrees from the University of Trondheim, Norway, in 1978 and 1992, respectively. From 1979 to 1983 he worked at the Division of Automatic control, SINTEF (the foundation of Scientific and Industrial Research) in Trondheim. Since 1983 he has been working at the Department of Biomedical Engineering, Faculty of Medicine, Norwegian University of Science and Technology. He is currently a research fellow, holding a stipend from the Norwegian Research Council. His research areas include stochastic signal/image processing with applications in ultrasonic imaging, Doppler and color flow imaging.